Available online at www.sciencedirect.com
ScienceDirect
Journal of Power Sources 169 (2007) 158–166
JOURNAL OF POWER SOURCES
www.elsevier.com/locate/jpowsour

# Steam reforming of ethanol at moderate temperature: Multifactorial design analysis of Ni/$La_2O_3$-$Al_2O_3$, and Fe- and Mn-promoted Co/ZnO catalysts ☆

José Antonio Torres [a,*], Jordi Llorca [b], Albert Casanovas [b], Montserrat Domínguez [b], Joan Salvadó [a], Daniel Montané [a]

[a] *Department of Chemical Engineering, Rovira i Virgili University, Av. Països Catalans 26, 43007 Tarragona, Spain*
[b] *Institut de Tècniques Energètiques, Universitat Politècnica de Catalunya, Diagonal 647, 08028 Barcelona, Spain*

Available online 30 January 2007

**Abstract**

Novel Co (10%) catalysts supported on ZnO and promoted with Fe and Mn (1%) were synthesized and characterized by high-resolution transmission electron microscopy (HRTEM), electron energy-loss spectroscopy (EELS), X-ray diffraction (XRD) and X-ray photoelectron spectra (XPS). Their catalytic activity for steam reforming of ethanol was compared with that of Ni catalysts supported on $La_2O_3$-$Al_2O_3$. Experiments at 400 and 500 °C, steam to carbon ratios of 2 and 4, and a wide interval of contact time were analyzed following a multifactorial experimental design. At 500 °C and a steam to carbon molar ratio of 4, complete conversion of ethanol was achieved above a contact time of 200 g min $mol^{-1}$ for all catalysts. The ratio of selectivity between hydrogen and methane was around 23 $mol_{H2}/mol_{CH4}$ in the Co catalysts, while it approached the thermodynamic equilibrium (5.7 $mol_{H2}/mol_{CH4}$) in the Ni catalysts. The Co catalysts do not promote methane-forming reactions like ethanol cracking and acetaldehyde decarbonilation, nor do they facilitate the reverse methane steam reforming reaction. The catalytic behavior of cobalt is enhanced by promotion with iron or manganese through the formation of bimetallic particles, which facilitates cobalt reducibility. This suggests that Co-Mn/ZnO and Co-Fe/ZnO catalysts have a good potential for their use for ethanol reforming at moderate temperature.


*Keywords:* Ethanol steam reforming; Hydrogen; Fuel cells; Nickel catalysts; Cobalt catalysts

## 1. Introduction

Developed societies face a critical need for higher efficiency in the production and consumption of energy, which is driven by the strain that the continuous rise in the demand and cost of fossil fuels is causing on the global economy, by the vulnerability and limitedness of oil and gas supplies in a mid-term future, and by global warming and environmental concerns [1–3]. In this context, fuel cells are envisaged to play a significant role as efficient devices to produce electric power, thus contributing to supply what current transformation technologies and fossil fuels alone will not be able to satisfy at an acceptable cost in the mid-term future [1,4], a context in which renewables are called to contribute significantly as a source of primary energy as well. Low temperature fuel cells (FC) are suitable for producing electrical power in portable devices, automobiles, and small and medium stationary power plants. Among the low temperature fuel cells, polymer electrolyte membrane fuel cells (PEMFC) have the highest efficiency, reliability, favorable power-to-weight ratio, and a fast start-up time [1,5]. The PEMFC uses hydrogen as fuel, its main drawback being the sensibility towards carbon monoxide. Current electrodes in the PEMFC require hydrogen with less than 10 ppm of carbon monoxide [1,6,7]. Therefore, the use of PEMFC needs of a dependable, efficient and flexible hydrogen supply that has to rely on stand-alone processes for the production of hydrogen (fuel processors) [8], preferably directly coupled to the PEMFC unit. Current concepts for fuel processors are based either on steam reforming (SR) or partial oxidation reforming (POXR) and they can use natural gas, LPG or oxygenated fuels. Alcohols are especially appealing as primary fuels for fuel processors because they can be obtained from renewable biomass: methanol trough gasification and synthesis, and ethanol trough fermentation. Ethanol is easier and

☆ This paper presented at the 2nd National Congress on Fuel Cells, CONAPPICE 2006.

* Corresponding author. Tel.: +34 977 558 556; fax: +34 977 558 544.
*E-mail address:* joseantonio.torres@urv.cat (J.A. Torres).

0378-7753/$ – see front matter © 2007 Elsevier B.V. All rights reserved.
doi:10.1016/j.jpowsour.2007.01.057

safer to store and transport due to its low toxicity and volatility, it is biodegradable, and since water is also consumed during its conversion into hydrogen, there is no need for absolute ethanol to be produced as it would be required if it were to be used in conventional engines, either alone or mixed with gasoline.

The development and testing of catalysts suitable for ethanol steam reforming has been recently reviewed [7,9]. Reported catalysts include oxide catalysts (ZnO, MgO, $V_2O_5$), metal-based catalysts on metal oxide supports (Ni/$Al_2O_3$, Ni/$La_2O_3$, Ni-Cu/$Al_2O_3$, Co/$Al_2O_3$, Co/ZnO) and some noble metal catalysts (Rh/$Al_2O_3$, Rh/MgO, Rh/$ZrO_2$, Rh/$CeO_2$-$ZrO_2$). The reaction pathway during ethanol steam reforming comprises a complex series of simultaneous reactions, which are more or less promoted depending on the nature of the catalyst [9–13]. Those include ethanol dehydration to ethylene, ethanol cracking into methane, carbon monoxide and hydrogen, ethanol dehydrogenation into acetaldehyde, acetaldehyde decarbonilation, ethanol decomposition into acetone, formation of acetic acid, steam reforming of ethanol, acetaldehyde, acetone, acetic acid, ethylene and methane, and the water gas shift and methanation reactions. Additionally, a major problem for ethanol steam reforming is the deposition of carbon by ethylene polymerization on the catalyst surface, and therefore suitable catalysts require combinations of active components and supports that do not promote dehydration and ethylene formation [9], and that are capable of reforming ethylene efficiently. Ethanol, however, decomposes through homogeneous thermal cracking into ethylene and water at high temperature [14]. The requirement for reduced carbon deposition on the catalyst as well as considerations about materials of construction and mechanical designs for fuel processors have driven research for obtaining catalysts that can reform ethanol efficiently and selectively at moderate and even low temperature, from 300 to 550 °C [15–19].

In this paper, we have conducted a systematic study to compare the activity and selectivity of two types of catalyst at moderate temperature and steam to carbon (S/C) ratios. Nickel-based catalysts (Ni/$La_2O_3$-$Al_2O_3$) and novel Co-based catalysts (Co-Fe/ZnO and Co-Mn/ZnO) have been prepared and tested at temperatures of 400 and 500 °C, steam to carbon (S/C) molar ratios of 2 and 4, and contact times from 4.3 to 1100 min $g_{cat}/mol_{EtOH}$, covering a range of ethanol conversion from 20 to 100%. A multifactorial design analysis has been conducted to establish the significance of temperature, S/C ratio, contact time and catalyst formulation on ethanol conversion and selectivity towards the different reaction products.

## 2. Experimental methods

### 2.1. Catalyst preparation and characterization

Two Ni/$La_2O_3$-$Al_2O_3$ catalysts were prepared by impregnation of La-stabilized alumina with a solution of $Ni(NO_3)_2{\cdot}6H_2O$ (Aldrich 99%). The resulting solids were calcined at 550 °C during 2 h and reduced at 550 °C for 5 h under a gas stream composed by 50% $H_2$ and 50% $N_2$ [20]. The La-stabilized alumina was prepared previously by impregnation of γ-alumina (150 mesh, Aldrich) with a solution of $La(NO_3){\cdot}6H_2O$ (Aldrich 99.99%) at room temperature for 1 h under stirring. The suspension was heated slowly up to 70 °C and maintained at this temperature to evaporate water, and the resulting solid was dried for 24 h at 105 °C and calcined in air at 900 °C during 30 h. The content of lanthanum metal was maintained constant at 8% by weight, and nickel metal content was set at 10 and 15% by weight. These catalysts were labeled as Ni10La08 and Ni15La08. Results from these Ni-based catalysts were compared with those of a commercial hydrocarbon steam reforming catalyst (ICI Katalco 46/1).

Catalysts based on cobalt were supported on ZnO and contained 10% of cobalt metal by weight and a 1% of Fe or Mn. They were prepared by co-precipitation at 30 °C by the addition of a $(NH_4)_2CO_3$ solution (0.6 M) to a mixture of $Zn(NO_3)_2$, $Co(NO_3)_2$, and $Fe(NO_3)_3$ or $Mn(NO_3)_2$ aqueous solutions ($[M^{x+}] = 0.8$ M). After aging for 2 h, the resulting solids were washed with distilled water, dried at 110 °C overnight, and calcined in air at 400 °C for 6 h. These catalysts were labeled as Co-Fe/ZnO and Co-Mn/ZnO. For comparative purposes a monometallic cobalt catalyst, Co/ZnO, was prepared in a similar way. Prior to the catalytic tests, these catalysts were reduced under hydrogen at 400 °C for 4 h.

BET surface areas were determined by nitrogen adsorption using a Micromeritics ASAP 2020 analyzer, and the metal surface was estimated by hydrogen chemisorption using a Micromeritics ASAP 2010 instrument. X-ray diffraction profiles (XRD) of the catalyst preparations were collected at a step width of 0.02° and by counting 10 s at each step with a Siemens D-500 instrument equipped with a Cu target and a graphite monochromator. Samples for high-resolution transmission electron microscopy (HRTEM) studies and electron energy-loss spectroscopy (EELS) were deposited on copper grids with a holey-carbon-film support. The instrument used was a JEOL JEM 2010F electron microscope equipped with a field emission electron source and operated at 200 kV. X-ray photoelectron spectra (XPS) were acquired with a Perkin-Elmer PHI-5500 spectrometer equipped with an Al X-ray exciting source and a hemispherical electron analyzer.

### 2.2. Catalytic tests

Catalysts were tested in a fixed-bed, laboratory-scale system described in detail elsewhere [21] that was modified to improve condensation and recovery of volatile products like acetaldehyde. The reactor was constructed with stainless-steel tube (15 mm inner diameter × 300 mm length) and had an axial thermocouple well (1/8 inch outer diameter), which housed three k-type thermocouples located at different positions along the length of the catalyst bed in order to check for temperature uniformity. Catalysts were sieved to 0.1–0.2 mm before testing. From 0.1 to 2.0 g of catalyst were diluted with 30 g of cordierite powder sieved to less than 0.5 mm to improve heat transfer and temperature homogeneity in the catalyst bed.

### 2.3. Experimental planning

A series of experiments was first developed at 500 °C and a steam to carbon (S/C) ratio of 4, changing the contact time

Table 1
Levels employed for the independent variables in the multifactorial experimental design

| Factor | Independent variable | Levels |
|---|---|---|
| A | Temperature (°C) | 400 and 500 |
| B | Catalyst | ICI 46/1 (20% Ni), Ni10La08 (10% Ni, 8% La), Ni15La08 (15% Ni, 8% La), Co-Mn/ZnO (10% Co, 1% Mn), Co/ZnO (10% Co), Co-Fe/ZnO (10% Co, 1% Fe) |
| C | S/C molar ratio | 2 and 4 |
| D | $W/F_{EtOH0}$ ($\min g_{cat}\ mol^{-1}$) | Test A: (Xa < 50%) 4, 6, 9, 33. Test B: (Xa > 50%) 150, 240, 460, 1100 |

($W/F_{EtOH0}$) to cover from low to complete conversion of ethanol. Additional experiments were then developed following a multifactorial experimental design to determine the variables that had a significant effect on ethanol conversion and selectivity towards reaction products. Temperature, catalyst formulation, S/C and contact time were the independent variables, and the response variables analyzed were ethanol conversion, and the selectivity to final ($H_2$, CO, $CO_2$, $CH_4$) and intermediate products ($C_2H_4$, $C_2H_6$, $C_2H_4O$, $C_2H_4O_2$). Table 1 shows the levels that were employed for each of the four independent variables. Ethanol conversion ($X$), selectivity towards the different products ($S_j$), ant their yields ($Yi_j$), were calculated according to Eqs. (1)–(3) where $F_j$ (mol $min^{-1}$) is the flow of species $j$ at the reactor exit and $F_{EtOH0}$ the flow rate of ethanol feed to the reactor.

$$X = \frac{F_{EtOH0} - F_{EtOH}}{F_{EtOH0}} \quad (1)$$

$$S_j = \frac{F_j}{\sum_{products} F_j} \quad (2)$$

$$Yi_j = \frac{F_j}{F_{EtOH0} - F_{EtOH}} \quad (3)$$

## 3. Results and discussion

### 3.1. Catalysts characterization

The Fe- and Mn-promoted cobalt catalysts prepared in this work (Co-Fe/ZnO and Co-Mn/ZnO) constitute novel cobalt-based catalysts and have been characterized in detail. After calcination at 400 °C, all catalysts showed by X-ray diffraction (XRD) the characteristic peaks of the $Co_3O_4$ spinel phase. In addition to ZnO peaks, no other signals appeared in the diffraction patterns of samples Co-Fe/ZnO and Co-Mn/ZnO. After reduction at 400 °C, peaks due to metallic cobalt (fcc) appeared in the XRD patterns of all catalysts and peaks due to $Co_3O_4$ disappeared. Since XRD did not provide information about the phases where the promoters were present, a detailed microstructural study was carried out on the reduced samples by combined high-resolution transmission electron microscopy and energy electron-loss spectroscopy (HRTEM-EELS) in order to determine if cobalt and promoter entities were in contact, or occurred as separate phases. This is important for elucidating the role of iron and manganese promoters in the catalytic behavior of these catalysts with respect to Co/ZnO.

Fig. 1 shows a representative lattice-fringe TEM image of the Co-Fe/ZnO catalyst along with Fourier Transform images (FT) of selected areas (labeled as A, B and C in the HRTEM image). Metallic particles (C in the image) of about 15–20 nm are well distributed over the ZnO support (A in the image). The EELS spectrum shown was recorded over the particle C alone. It shows the simultaneous presence of cobalt and iron, with an approximate Co:Fe atomic ratio of 9:1, which corresponds well with the cobalt and iron content by weight of the sample. All individual metallic particles analyzed by EELS in the catalyst gave similar results. The FT image of the metallic particle C exhibits strings indicative of structural disorder along the [1 1 1] crystallographic direction, which is also visible in direct space in the HRTEM image at high magnification. It can be concluded from EELS spectra and FT images that the Co-Fe/ZnO catalyst is constituted by alloy particles. In addition, these alloy particles

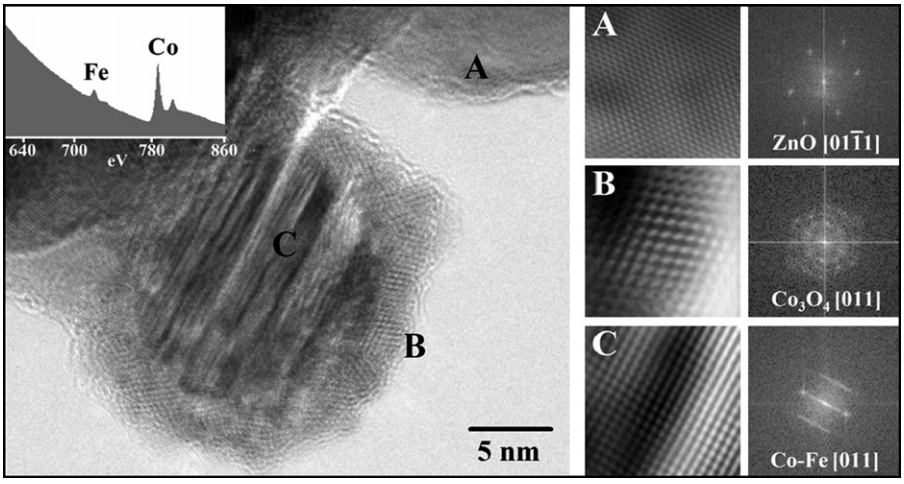


Fig. 1. High-resolution transmission electron microscopy image of catalyst Co-Fe/ZnO. Lattice-fringe analysis, EELS spectra and FT images indicate that the catalyst contains bimetallic Co-Fe particles. (A) ZnO support, (B) $Co_3O_4$ and (C) bimetallic Co-Fe.

Table 2
X-ray photoelectron spectroscopy data obtained for cobalt-based catalysts after reduction at 673 K

| Catalyst | $Co_{at}/Zn_{at}$ | $M_{at}/Co_{at}$ | $\%Co^0$ | $\%Co^{\delta+}$ |
|---|---|---|---|---|
| Co/ZnO | 0.27 | n.a. | 30 | 70 |
| Fe-Co/ZnO | 0.22 | 0.25 | 46 | 54 |
| Mn-Co/ZnO | 0.21 | 0.34 | 51 | 49 |

are sometimes covered by a thin layer of $Co_3O_4$ (B in the image), with distinctive lattice spacing at 4.67 and 2.86 Å corresponding to (1 1 1) and (2 2 0) planes, respectively.

Fig. 2 corresponds to the Co-Mn/ZnO sample. Again, metallic particles of about 15–20 nm (B and C in the HRTEM image) are well dispersed over ZnO (A in the image). This size distribution is also similar to reference sample Co/ZnO [18]. EELS spectra recorded over individual metallic particles show in all cases the common occurrence of cobalt and manganese, with Co:Mn atomic ratios of about 9:1, in accordance to metal loadings of the catalyst. The FT images corresponding to different areas of the metallic particle shown in Fig. 2 depict strings in various crystallographic directions (B and C in the figure) which is indicative of structural disorder due to the incorporation of manganese into the fcc structure of metallic cobalt. Therefore, catalyst Co-Mn/ZnO is constituted by bimetallic particles, too. However, in contrast to Co-Fe/ZnO, most of the alloy particles in the Co-Mn/ZnO catalyst are not covered by any cobalt oxide layer visible by HRTEM.

X-ray photoelectron spectroscopy (XPS) was also used for the study of cobalt-based catalysts with the purpose of determining the surface composition of catalysts and the effect of promoters on the reducibility of cobalt, since it has been reported that the redox pair $Co^0/Co^{2+}$ is responsible for the catalytic behavior of cobalt-based catalysts in the ethanol steam reforming reaction [22]. Table 2 reports the XPS data recorded for the three cobalt catalysts used in this work. From both the Co/Zn and M/Co atomic values, it is deduced that the cobalt dispersion is similar in all cases. This is also in accordance to the similar particle size values obtained from TEM. On the other hand, there is a strong surface segregation of the promoters Fe and Mn ($M_{at}/Co_{at}$ = 0.25–0.34 compared to the bulk value of 0.1). Finally, there is a clear effect of the promoters on the surface reducibility of cobalt. The amount of metallic cobalt increases from 30 up to ca. 50% when iron or manganese are present in the catalyst formulation. This may likely have a strong effect on the catalytic performance of promoted, cobalt-based catalysts. The different values of surface $\%Co^0$ and $\%Co^{\delta+}$ between Co-Fe/ZnO and Co-Mn/ZnO may be related to the presence of the $Co_3O_4$ spinel layer around the bimetallic particles in the former as determined by HRTEM.

The characteristics of the nickel-based catalyst used in this work have been reported in the literature and, consequently, are not discussed here. Briefly, from XRD results it has been shown that Ni particles with a mean diameter of 33 nm are found to be stabilized over the $La_2O_3$ support [23], and Ni particles of 15 nm are encountered over $\gamma$-$Al_2O_3$ [24]. BET surface areas were between 33 and 51 $m^2\,g^{-1}$ and metal dispersion in the fresh catalysts calculated from chemisorption experiments were 3.0–4.1%.

### 3.2. Catalytic tests

In the first series of experiments, two nickel-based catalysts (Ni15La08 and commercial ICI 46/1) and two Co catalysts (Co-Fe/ZnO and Co-Mn/ZnO) were tested at 500 °C under a S/C molar ratio of 4, varying the contact time in order to cover conditions from low to complete ethanol conversion. Fig. 3 shows that complete ethanol conversion was achieved for all catalysts at a contact time above 200 g min $mol^{-1}$, except for the ICI catalyst. Hydrogen yield is also shown in Fig. 3 and exhibits a distinct behavior between the two types of catalysts. Both Co catalysts follow the same evolution with contact time. At short contact time, they produce less than 1.5 mol of hydrogen per mol of ethanol consumed, but hydrogen yield reaches around 4.3 $mol_{H2}/mol_{EtOH}$ once the conversion of ethanol is complete at higher contact times. The Ni-based catalysts, on the con-

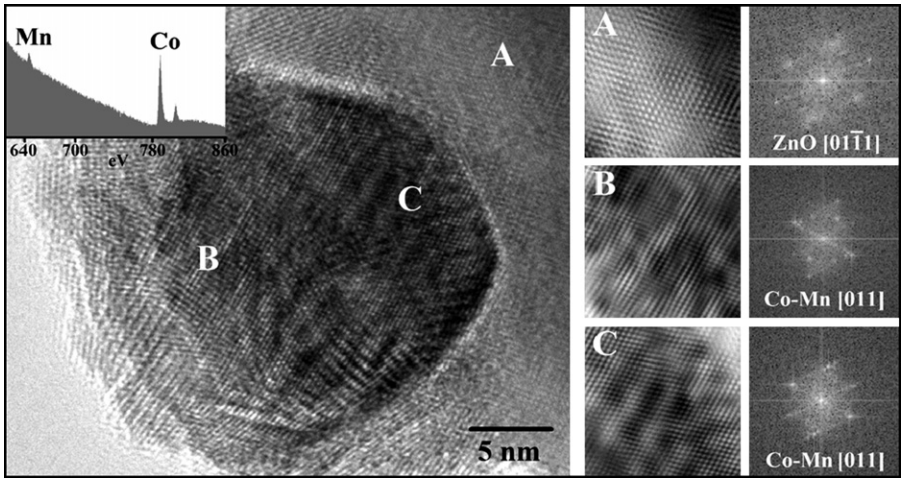


Fig. 2. High-resolution transmission electron microscopy image of catalyst Co-Mn/ZnO. Lattice-fringe analysis, EELS spectra and FT images indicate that the catalyst contains bimetallic Co-Mn particles. (A) ZnO support, (B and C) bimetallic Co-Mn.

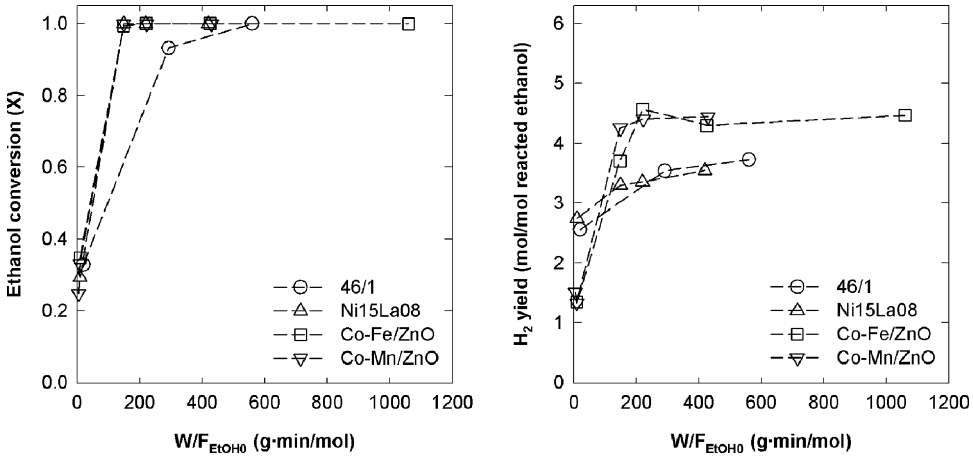


Fig. 3. Variation of ethanol conversion and hydrogen yield with contact time for Ni and Co based catalyst (S/C = 4, $T$ = 500 °C and atmospheric pressure. Dashed lines only indicate trends).

trary, had a higher yield at short contact time but it tended to stabilize around 3.6 $mol_{H2}/mol_{EtOH}$ at complete ethanol conversion. The evolution of selectivity with contact time towards intermediate ($C_2H_4$, $C_2H_6$, $C_2H_4O$ and $C_2H_4O_2$), and final products ($H_2$, CO, $CO_2$ and $CH_4$) for the Ni catalysts is shown in Fig. 4. Acetaldehyde and ethylene were the main intermediate products, although they were only present at the lower contact time when ethanol conversion was still incomplete. Selectivity towards acetaldehyde was lower in the Ni15La08 catalyst, which suggests that it does not promote ethanol dehydrogenation as much as the commercial catalyst, or that it is more efficient in reforming acetaldehyde. The latter agrees with the

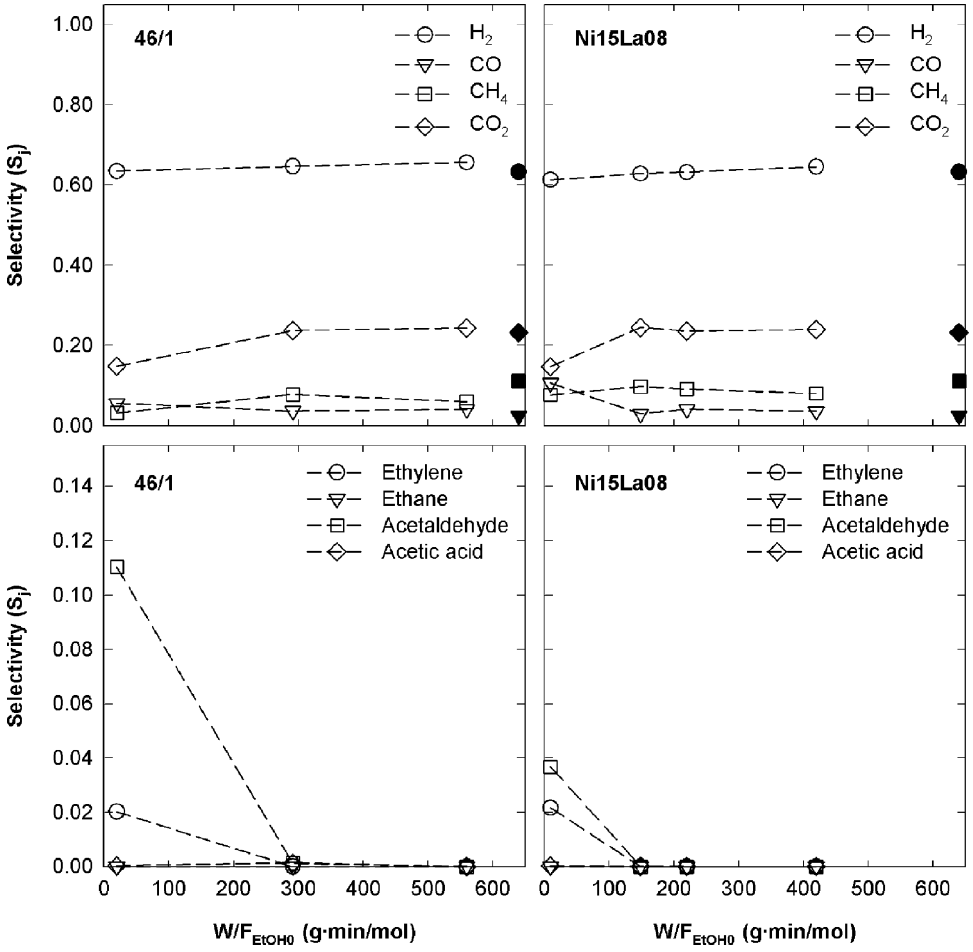


Fig. 4. Variation of the selectivity towards reaction products with contact time for Ni-based catalyst (S/C = 4, $T$ = 500 °C and atmospheric pressure. Solid symbols show equilibrium selectivities. Dashed lines only indicate trends).

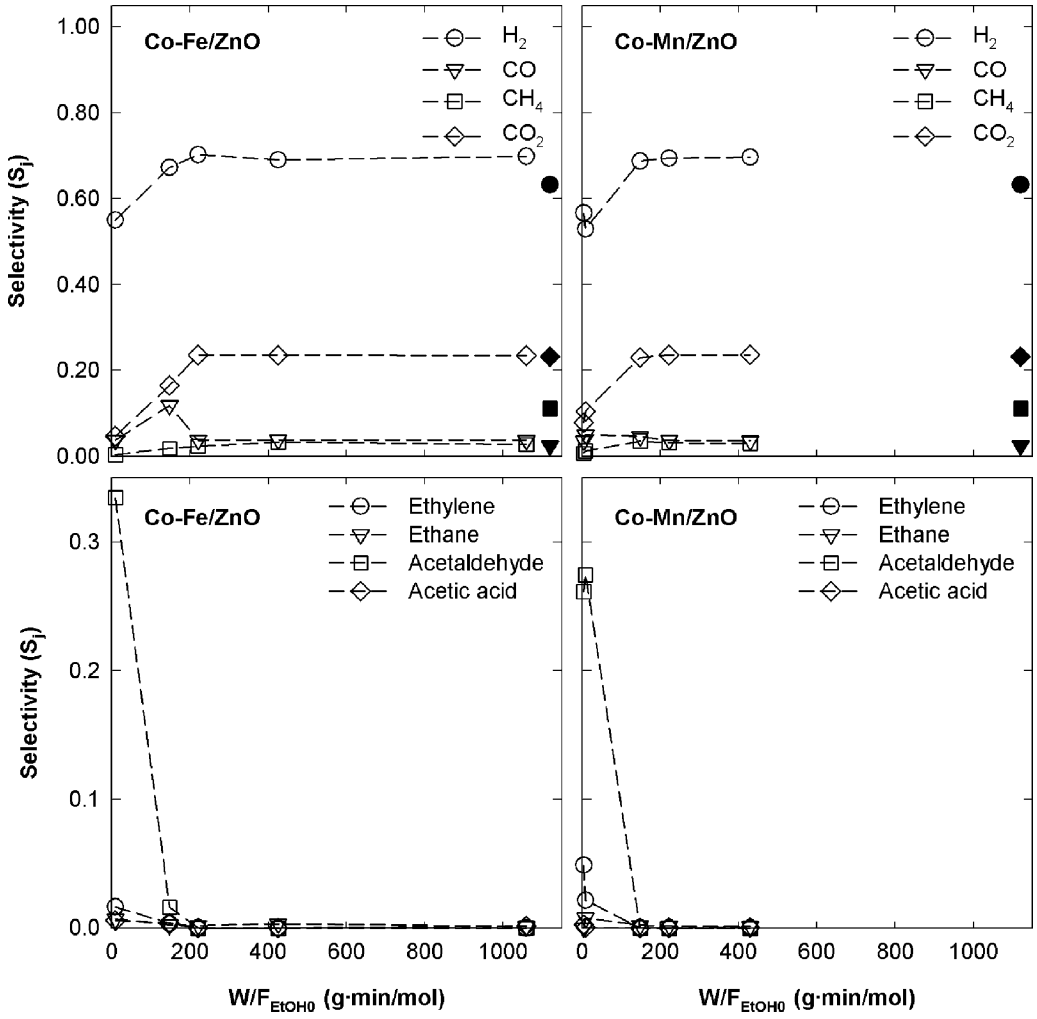


Fig. 5. Variation of the selectivity towards reaction products with contact time for Co based catalyst (S/C = 4, $T$ = 500 °C and atmospheric pressure. Solid symbols show equilibrium selectivities. Dashed lines only indicate trends).

higher conversion obtained with the Ni15La08 catalyst, even at low contact time. Selectivity towards ethylene was equivalent for both catalysts. The variation of the selectivity towards final products with contact time was very similar in both cases. At short contact time they produced more CO than $CH_4$ but this reversed at contact times above 100 g min mol$^{-1}$, when the selectivity of the four products tended to the thermodynamic equilibrium. Results of the Co-based catalysts are shown in Fig. 5, and some distinctive trends are observed. Trace amounts of secondary products including ethane, which was not detected in the Ni catalysts, were detected in the gas for both catalysts even at a contact time of 1060 g min mol$^{-1}$ for the Co-Fe/ZnO catalyst. The Co-Fe/ZnO catalyst produced more acetaldehyde than the Co-Mn/ZnO at low contact time, indicating that it may be more active in ethanol dehydrogenation, and also produced more CO but less ethylene. At high contact times, $S_j$ for the final products tended to the same limit values for both catalysts. Hydrogen selectivity stabilized at around 0.69 and methane at 0.029, which differ substantially from their respective equilibrium values of 0.63 and 0.11, although CO and $CO_2$ were close to equilibrium. Fig. 6 plots the ratio of selectivity

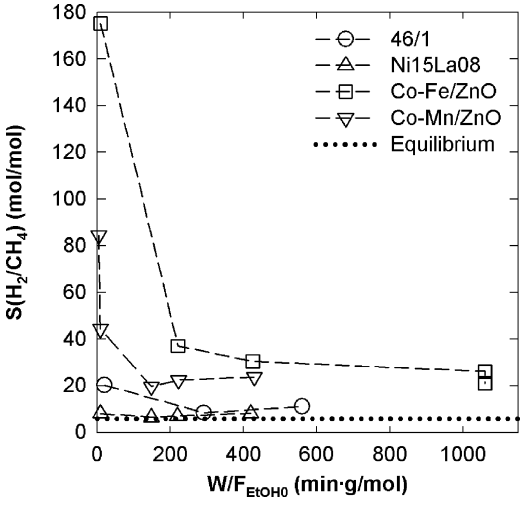


Fig. 6. Variation of the ratio of selectivity between $H_2$ and $CH_4$, S($H_2$/$CH_4$) with contact time, for the Ni and Co catalysts (S/C = 4, $T$ = 500 °C and atmospheric pressure).

Table 3
Main reactions involved in the catalytic steam reforming of ethanol from Refs. [7,9,13]

| | | | s. eq. # |
|---|---|---|---|
| Decomposition reactions | | | |
| Ethanol | $CH_3CH_2OH \leftrightarrows CH_3CHO + H_2$ | Dehydrogenation | 1 |
| | $CH_3CH_2OH \rightarrow CH_2{=}CH_2 + H_2O$ | Dehydration | 2 |
| | $CH_3CH_2OH \rightarrow CO + CH_4 + H_2$ | Cracking | 3 |
| | $CH_3CH_2OH + H_2O \rightarrow CH_3COOH + 2H_2$ | Oxidation | 4 |
| Acetaldehyde | $2CH_3CHO \rightarrow CH_3COCH_3 + CO + H_2$ | Acetone formation | 5 |
| | $CH_3CHO \rightarrow CO + CH_4$ | Decarbonilation | 6 |
| Acetic | $CH_3COOH \rightarrow CO_2 + CH_4$ | Decarboxilation | 7 |
| Ethylene | $CH_2{=}CH_2 \rightarrow 2C + 2H_2$ | Carbon deposition | 8 |
| Methane | $CH_4 \rightarrow C + 2H_2$ | Carbon deposition | 9 |
| Carbon monoxide | $2CO \leftrightarrows C + CO_2$ | Carbon deposition | 10 |
| Steam reforming reactions | | | |
| Ethanol | $CH_3CH_2OH + H_2O \rightarrow 2CO + 4H_2$ | | 11 |
| Acetaldehyde | $CH_3CHO + H_2O \rightarrow 2CO + 3H_2$ | | 12 |
| Acetic | $CH_3COOH + 2H_2O \rightarrow 2CO_2 + 4H_2$ | | 13 |
| Acetone | $CH_3COCH_3 + 2H_2O \rightarrow 3CO + 5H_2$ | | 14 |
| Ethylene | $CH_2 = CH_2 + 2H_2O \rightarrow 2CO + 4H_2$ | | 15 |
| Methane | $CH_4 + H_2O \leftrightarrows CO + 3H_2$ | | 16 |
| Carbon monoxide | $CO + H_2O \leftrightarrows CO_2 + H_2$ | Water gas shift | 17 |
| Carbon | $C + H_2O \leftrightarrows CO + H_2$ | Carbon gasification | 18 |

between hydrogen and methane $S(H_2/CH_4)$ with contact time and it shows that Co-based catalysts consistently gave higher selectivity towards hydrogen that Ni catalysts, and that it stabilized at around 23 $mol_{H2}/mol_{CH4}$, while the equilibrium value was only 5.7 $mol_{H2}/mol_{CH4}$. This shows that the Co-based catalysts we synthesized in this work are not active for catalyzing the formation of methane.

Additional experiments at low ethanol conversion were performed at S/C ratios of 2 and 4 and temperatures of 400 and 500 °C in order to determine the reactions pathways promoted by the different families of catalysts. Three Ni- (Ni10La08, Ni15/La08 and commercial ICI 46/1), and three Co-based catalysts (Co/ZnO, Co-Fe/ZnO and Co-Mn/ZnO) were tested. The reaction pathway during ethanol catalytic steam reforming comprises a complex series of simultaneous reactions [9–13], which are more or less promoted depending on the nature of the catalyst and the reaction conditions. A general set of stoichiometric equations (s. eq.) for the reactions is summarized in Table 3 grouped into decomposition reactions, and steam reforming reactions where water takes an active role. Decomposition reactions include ethanol dehydrogenation to acetaldehyde, ethanol and acetaldehyde cracking into methane, carbon monoxide and hydrogen, acetaldehyde decarbonilation, acetaldehyde decomposition into acetone, ethanol dehydration to ethylene, formation of acetic acid and decarboxilation of acetic acid. Those reactions produce carbon oxides, methane, hydrogen and intermediate species that will react subsequently with water on the catalyst surface through the steam reforming reactions of ethanol, acetaldehyde, acetone, acetic acid and ethylene, to yield hydrogen, methane, and carbon oxides. The latter tend to thermodynamic equilibrium through the methane steam reforming and the water gas shift, provided that the catalyst promotes those reactions and the contact time is high enough. However, decomposition reactions that lead to the deposition of carbon (coking) on the surface of the catalyst are also possible, mainly from ethylene polymerization.

Fig. 7 shows the molar yield of the different reaction products for Ni catalysts at 400 and 500 °C, and a S/C ratio of 4. At 400 °C, the dehydrogenation of ethanol to acetaldehyde (s. eq. 1) was the main reaction for the Ni catalysts, and ethanol and acetaldehyde reforming (s. eqs. 11 and 12) were less favored, as deduced from the low yields of carbon oxides. When temperature was raised to 500 °C, steam reforming reactions become predominant and the yields of $H_2$ and $CO_2$ raised substantially while the yield of acetaldehyde was reduced, especially for the Ni/La catalysts. The Ni15La08 catalyst produced more CO and $CH_4$ than the Ni10La08, which suggests that it is more active for cracking reactions (s. eqs. 3 and 6). Finally, ethylene formation was similar at both temperatures, and ethane and acetic acid were not detected at significant concentrations. Data under the same experimental conditions is reported in Fig. 8 for Co catalysts. At 400 °C, the Co-Fe/ZnO catalyst had almost the same yield of hydrogen and acetaldehyde, and CO and $CO_2$ were produced at lower, but similar, concentrations. Little methane and ethylene were detected, which shows that ethanol was consumed mainly through dehydrogenation (s. eq. 1). Acetaldehyde was converted through steam reforming (s. eq. 12), and $CO_2$ was formed through the shift reaction (s. eq. 17). At 500 °C, this catalyst showed the same behavior and $H_2$ and CO yields were larger. The Co-Mn/ZnO catalyst was more active for steam reforming reactions, with higher yields of hydrogen and carbon dioxide, while the Co/ZnO had an intermediate behavior, depending on temperature. For all Co catalysts, methane production was very low, even below the formation of ethylene at 400 °C, which demonstrated that this family of catalysts has little activity for ethanol and acetaldehyde cracking (s. eqs. 3 and 6), and the for-

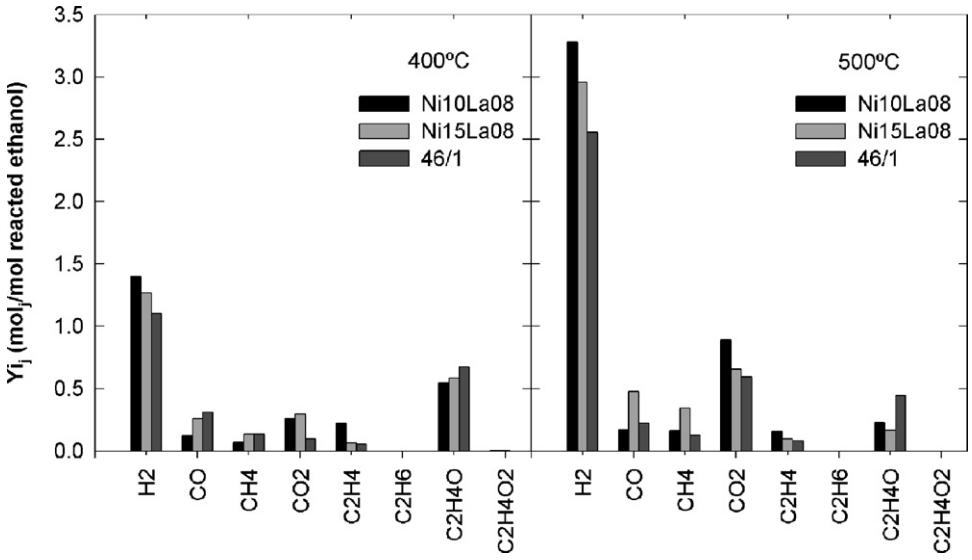


Fig. 7. Yields of products formed per mol of ethanol consumed at 400 and 500 °C for the Ni catalysts (S/C = 4, $W/F_{EtOH0}$ = 9 g min $mol^{-1}$, atmospheric pressure).

mation of methane through the reverse methane steam reforming (s. eq. 9). Ethane and acetic acid were detected at low concentrations for the three catalysts. The effect of Fe and Mn in the catalytic performance of catalysts Co-Fe/ZnO and Co-Mn/ZnO with respect to Co/ZnO may be explained due to the presence of bimetallic particles, which in turn affect cobalt reducibility. In particular, Co-Mn entities appear to be highly effective for steam reforming reactions at 500 °C, where hydrogen yield is maximum.

Variance analyses of the results obtained from the series of experiments carried out at low and high ethanol conversion were performed in order to identify the variables that had a significant effect on the conversion of ethanol and the selectivity towards products at the 95% of probability level. From the data set of low ethanol conversion experiments, it is concluded that the most important factor is the catalyst formulation, which has a significant effect on ethanol conversion and selectivity towards all products (Table 4). Temperature has a significant effect on conversion and selectivity towards $H_2$ and $CO_2$, and contact time ($W/F_{EtOH0}$) affects conversion, and hydrogen and methane selectivities. The second set of experiments analyzed were those covering ethanol conversions above 50%, which were all performed at constant temperature (500 °C) and S/C molar ratio (4) but varying catalyst type and contact time. In this case, from Table 5, we conclude that contact time has a negligible effect in the interval studied. The catalyst type has a significant effect on the selectivity towards hydrogen and methane, but the selectivity towards carbon oxides are equivalent regardless of the catalyst type. These results are consistent with the different reaction pathways promoted by each type of catalyst, and show that the reaction over the novel Co-Mn/ZnO and Co-Fe/ZnO catalysts proceeds mainly by ethanol dehydrogenation, acetaldehyde steam reforming, and water gas shift reactions. In contrast to Ni-based catalysts, ethanol and acetaldehyde cracking reactions are

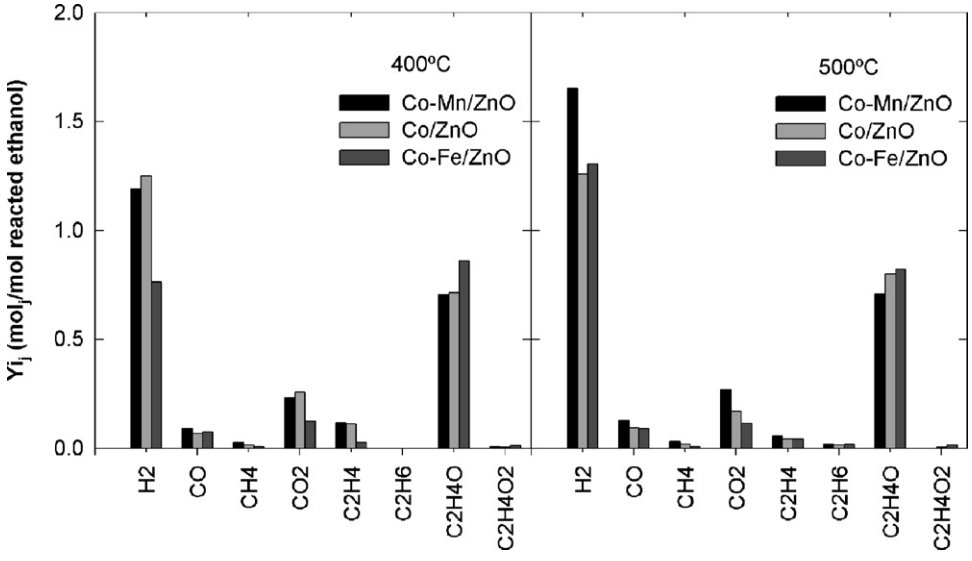


Fig. 8. Yields of products formed per mol of ethanol consumed at 400 and 500 °C for the Co catalysts (S/C = 4, $W/F_{EtOH0}$ = 9 g min $mol^{-1}$, atmospheric pressure).

Table 4
Factor and interaction effects corresponding to the factorial design at low ethanol conversion

| Factor | $X_{EtOH}$ | Selectivity | | | | | | |
|---|---|---|---|---|---|---|---|---|
| | | $H_2$ | CO | $CH_4$ | $CO_2$ | $C_2H_4$ | $C_2H_4O$ | $H_2/CH_4$ |
| A (temperature) | × | × | | | × | | | |
| B (catalyst type) | × | × | × | × | × | × | × | × |
| C (S/C) | × | | | | | | | |
| D ($W/F_{EtOH0}$) | × | × | | × | | | | × |
| AB | | × | | | × | | | |
| AC | | | | | | | | |
| AD | | × | × | | | | | |

Symbol (×) indicates a significant influence at 95% of probability.

Table 5
Factor and interaction effects corresponding to the factorial design at high ethanol conversion

| Factor | $X_{EtOH}$ | Selectivity | | | | |
|---|---|---|---|---|---|---|
| | | $H_2$ | CO | $CH_4$ | $CO_2$ | $H_2/CH_4$ |
| B (catalyst type) | | × | | × | | × |
| D ($W/F_{EtOH0}$) | | | | | | |
| BD | | | | | | |

Symbol (×) indicates a significant influence at 95% of probability.

almost suppressed over Co-based catalysts, as demonstrated by their very low selectivity towards methane formation. The same applies for the reverse methane steam reforming reaction since methane formation is always well below the thermodynamic equilibrium, even at extended contact times.

## 4. Conclusions

The Co- and Ni-based catalyst that we have tested are active for the steam reforming of ethanol at a moderate temperature, from 400 to 500 °C, and steam to carbon molar ratios from 2 to 4. For Ni-based catalysts, ethanol dehydrogenation dominate at low temperature, but steam reforming reactions become dominant at 500 °C. Upon complete conversion of ethanol and acetaldehyde, the distribution of final products approaches chemical equilibrium, which denotes that these catalysts are active for the water shift and methane steam reforming equilibrium reactions as well. The Co-based catalysts favor ethanol dehydrogenation into acetaldehyde, which is then converted through steam reforming. The reversible shift reaction is also promoted by these catalysts and the relationship among the yields of carbon oxides approaches that of equilibrium. On the contrary, these catalysts do not promote methane-forming reactions like ethanol cracking and acetaldehyde decarbonilation, nor they facilitate the reverse methane steam reforming reaction. This results on a final product in which the ratio between hydrogen and methane selectivity is well above equilibrium. The catalytic behavior of cobalt is enhanced by promotion with iron or manganese through the formation of bimetallic particles, which facilitates cobalt reducibility. This suggests that Co-Mn/ZnO and Co-Fe/ZnO catalysts have a good potential for their use in fuel processors for ethanol reforming that operate at moderate temperature.

## Acknowledgments

The authors are indebted for financial support to DURSI (Catalan Regional Government Project 2005SGR-00580) and the Spanish Government (Projects CTQ2005-09182-C02-01/PPQ and ENE2006-06925, both partially funded by the FEDER program of the European Union). J.A. Torres is grateful to the Rovira i Virgili University for his Ph.D. scholarship.

## References

[1] C. Song, Catal. Today 77 (2002) 17–49.
[2] H. Turton, L. Barreto, Energy Policy 34 (2006) 2232–2250.
[3] P. Hennicke, M. Fischedick, Energy Policy 34 (2006) 1260–1270.
[4] W. McDowall, M. Eames, Energy Policy 34 (2006) 1236–1250.
[5] V. Fierro, O. Akdim, H. Provendier, C. Mirodatos, J. Power Sources 145 (2005) 659–666.
[6] V. Klouz, V. Fierro, P. Denton, H. Katz, J.P. Lisse, S. Bouvot-Mauduit, C. Mirodatos, J. Power Sources 105 (2002) 26–34.
[7] P.D. Vaidya, A.E. Rodrigues, Chem. Eng. J. 117 (2006) 39–49.
[8] G. Kolios, B. Glöckler, A. Gritsch, A. Morillo, G. Eigenberger, Fuel Cells 5 (2005) 52–65.
[9] A. Haryanto, S. Fernando, N. Murali, S. Adhikari, Energy Fuels 19 (2005) 2098–2106.
[10] S. Cavallaro, V. Chiodo, S. Freni, N. Mondillo, F. Frusteri, Appl. Catal. A 249 (2003) 119–128.
[11] F. Frusteri, S. Freni, L. Spadaro, V. Chiodo, G. Bonura, S. Donato, S. Cavallaro, Catal. Commun. 5 (2004) 611–615.
[12] N. Fatsikostas, X.E. Verykios, J. Catal. 225 (2004) 439–452.
[13] M. Benito, J.L. Sanz, R. Isabel, R. Padilla, R. Arjona, L. Daza, J. Power Sources 151 (2005) 11–17.
[14] Li, A. Kazakov, F.L. Dryer, Int. J. Chem. Kinet. 33 (2001) 859–867.
[15] J. Sun, X. Qiu, F. Wu, W. Zhu, W. Wang, S. Hao, Int. J. Hydrogen Energy 29 (2004) 1075–1081.
[16] J. Sun, X. Qiu, F. Wu, W. Zhu, Int. J. Hydrogen Energy 30 (2005) 437–445.
[17] J. Llorca, N. Homs, J. Sales, P. Ramírez de la Piscina, J. Catal. 209 (2002) 306–317.
[18] J. Llorca, P. Ramírez de la Piscina, J.A. Dalmon, J. Sales, N. Homs, Appl. Catal. B 43 (2003) 355–369.
[19] J. Llorca, N. Homs, J. Sales, J.-L.G. Fierro, P. Ramírez de la Piscina, J. Catal. 222 (2004) 470–480.
[20] A.N. Fatsikostas, D.I. Kondarides, X.E. Verykios, Catal. Today 75 (2002) 145–155.
[21] M. Marquevich, R. Coll, D. Montané, Ind. Eng. Chem. Res. 39 (2000) 2140–2147.
[22] J. Llorca, J.-A. Dalmon, P. Ramírez de la Piscina, N. Homs, Appl. Catal. A 243 (2003) 261–269.
[23] X.E. Verykios, Int. J. Hydrogen Energy 28 (2003) 1045–1063.
[24] G. Li, L. Hu, J.M. Hill, Appl. Catal. A 301 (2006) 16–24.